

# Simulation of an isothermal hydrodesulfurization small reactor with different catalyst particle shapes

M.J. Macías<sup>a,b</sup>, J. Ancheyta<sup>a,b,\*</sup>

<sup>a</sup>*Instituto Mexicano del Petróleo, Eje Central Lázaro Cárdenas 152, México, D.F. 07730, México*

<sup>b</sup>*Escuela Superior de Ingeniería Química e Industrias Extractivas (ESIQIE-IPN),  
UPALM, Zacatenco, México, D.F. 07738, México*

## Abstract

In this work we examine the effect of different catalyst particle shapes (sphere, pellet, cylinder, 2-lobe, 3-lobe, and 4-lobe) on the characteristics and behavior of hydrodesulfurization catalyst and reactor, such as liquid holdup, external and internal concentration gradients, sulfur content in the product, and pressure drop. The analysis was based on experimental information obtained in a small hydrodesulfurization reactor using straight-run gas oil as feed and a tri-lobular commercial catalyst sample at typical commercial operating conditions. An isothermal reactor model is described in detail, which was validated with experimental information and then applied to study the effect of the different particle shapes on HDS reaction.

© 2004 Elsevier B.V. All rights reserved.

**Keywords:** Hydrodesulfurization; Modeling; Catalyst shape

## 1. Introduction

In the petroleum refining industry, hydrodesulfurization (HDS) of middle distillates is commonly accomplished in trickle-bed reactors in which three phases, gas (mostly hydrogen), liquid (oil) and solid catalyst particles are present. The conventional HDS process is usually conducted over sulfided CoMo/ $\gamma$ -Al<sub>2</sub>O<sub>3</sub> and NiMo/ $\gamma$ -Al<sub>2</sub>O<sub>3</sub> catalysts. Diffusion characteristics, pressure drop limitations, catalyst pore size, catalyst loading techniques, and catalytic activity requirements all affect the selection of the catalyst shape used in HDS reactors. Hence, to improve catalyst performance all steps in the catalyst preparation should be taken into account [1].

Extrudate particles are the preferred catalyst shape for middle distillate HDS processes. Small catalyst particles ranging 1/20–1/8 in diameter have demonstrated that pore diffusion limitation plays an important role in commercial application, however, the use of smaller particles is

impracticable because of the strong increase of the pressure drop in the catalyst bed. With non-cylindrical extrudate particles relatively low pressure drop might be achieved since they have a high external area to volume ratio, moreover, they exhibit better diffusion performance. On the other hand large particles often have low activity and cause low pressure drop. Therefore, a good selection of particle size and shape has to be made depending on the type of feedstock and operating conditions in order to optimize catalyst behavior [2–4].

Various experimental and theoretical studies of the effect of shape, size, loading, etc. of catalytic particles on HDS catalyst behavior have been reported in the literature [1–6]. Very nice and deep discussions have been made in order to correlate catalyst shape and size, particle size distribution, catalyst bulk density, catalyst pretreatment, diluent size, loading techniques, etc. with catalyst activity and bed characteristics.

de Bruijn et al. [2] presented an investigation of the effects of non-cylindrical shape of extrudates on the HDS of oil fractions, and reported that for a particle volume identical with that of cylindrical extrudates, non-cylindrical

\* Corresponding author. Tel.: +52 55 9175 8443; fax: +52 55 9175 8429.  
E-mail address: [jancheyt@imp.mx](mailto:jancheyt@imp.mx) (J. Ancheyta).

**Nomenclature**

$a_t$	liquid–solid interfacial area per unit volume of reactor
A	component sulfur
B	component hydrogen
$C_A$	molar concentration of A in product
$C_{AL}$	molar concentration of A in the liquid
$C_{AS}$	molar liquid phase of A inside the solid
$d_p$	particle diameter
$d_{peq}$	equivalent particle diameter
$d_{15.6}$	specific gravity at 15.6 °C
$D_A$	diffusion coefficient of A in the liquid phase
$D_{eff}$	effective diffusivity of A in the pores of catalyst
$D_{kA}$	Knudsen diffusivity
$D_R$	reactor diameter
g	gas phase
$G_L$	liquid superficial flow
k	reaction rate coefficient
$k_{ap}$	apparent kinetic constant
$k_L$	gas–liquid mass transfer coefficient
$k_s$	liquid–solid mass transfer coefficient
L	liquid phase
$L_B$	bed height
LHSV	liquid hourly space velocity
$L_p$	length particle
n	reaction order
P	pressure
$\Delta P_g$	frictional pressure drop, for gas flow only
$\Delta P_{gL}$	two-phase frictional pressure drop
$\Delta P_i/L_B$	frictional pressure drop per unit bed height with only liquid or gas flowing
$\Delta P_L$	frictional pressure drop, for liquid flow only
PM	molecular weight
$r_c$	radius of cylinder
$r_g$	mean pore radius
R	gas law constant
$Re_L$	liquid reynolds number
$S_g$	specific surface area of particle
$S_p$	total geometric external area of particle
T	temperature
$T_{MeABP}$	mean average boiling point
$u_i$	superficial velocity of the liquid or gas phase in the reactor
$u_L$	superficial velocity of the liquid
$v_A$	molar volume of solute A
$v_L$	molar volume of liquid solvent
$V_g$	pore volume per unit mass of catalyst
$V_p$	total geometric volume of catalyst

**Greek symbols**

$\varepsilon_B$	bed void fraction
$\varepsilon_L$	liquid holdup
$\eta$	effectiveness factor

$\theta$	particle porosity
$\mu_i$	viscosity of the liquid or gas phase
$\mu_L$	liquid viscosity
$\rho_B$	catalyst bulk density
$\rho_i$	density of the liquid or gas
$\rho_L$	liquid density
$\rho_p$	particle density
$\sigma$	collision diameter
$\tau$	tortuosity
$\nu_A$	stoichiometric coefficient of A
$\nu_B$	stoichiometric coefficient of B
$\nu_p$	stoichiometric coefficient of product
$\nu_c^m$	critical specific volume of the liquid
$\nu_{ci}^m$	critical specific volume of the liquid or gas
$\phi$	Thiele modulus
$\Omega$	collision integral

extrudates may lead to an activity which is higher than that of the cylindrical ones, depending on the degree of diffusion limitation.

Cooper et al. [1] reported the effect of different hydrotreating conditions on various shapes of NiMo catalysts and recommended that an integrated approach should be considered in which aspects of size, shape, pore size and catalyst loading must be taken into account for better design of HDT catalysts. They also recognized that it is not possible to select a single catalyst shape as the best choice in all hydrotreating applications.

Carruthers and Dicamillo [3] have described the influence of catalyst moisture content, catalyst particle size distribution, catalyst bulk density, presulfiding, catalyst shape and loading effects on the hydrodesulfurization and hydrodenitrogenation of several commercial catalysts. Their main findings were:

- HDS and HDN activities generally decrease with increasing moisture content of the catalyst.
- Long particles in pilot scale units often distort results due to holdup/channeling effects.
- Presulfiding at low temperatures is seen to lower overall conversion but does not change catalyst rankings appreciable.
- Variations in loadings patterns have less effect on final conversion than does the use of small particle size inert diluent.

Bej [7] has reviewed the various reactors and approaches that have been used at different stages of hydrotreating catalysts research and process development. He concluded that initial catalyst screening experiments can be conducted either in a batch autoclave or in a continuously operated fixed bed micro-reactor. He also emphasized that selection of diluent size is very important and depends on several factors such as length and diameter of the reactor, and on size and shape of the catalyst.

The common way employed in the literature to look on the effect of particle shape is to compare activity as a function of total geometric volume to external area of the catalyst particle ( $V_p/S_p$ ). This definition of particle size, firstly proposed by Aris [8] for spheres, cylinders, and flat plats, can also be used to other non-cylindrical catalyst particles [9].

Most of the reported work has been conducted experimentally in different reactor scales, which is certainly the best method to do this type of studies, however, the use of experimental reactor modeling and simulation for this purpose has not received too much attention, and by this approach more complete and interesting information could be obtained.

This contribution is an attempt to study the effect of different particle shapes on catalyst behavior during hydrodesulfurization of straight-run gas oil by using computer simulation.

## 2. Description of the reactor model

### 2.1. Assumptions

The following assumptions were considered for formulating the reactor model:

- Isothermal and steady-state operation.
- Catalyst deactivation is insignificant.
- The reaction is assumed to occur only into porous solid catalyst uniformly wetted by the liquid.
- Radial and axial concentration gradients are negligible.
- Kinetics of HDS reaction is described by a power-law model.
- Gas and liquid velocities are constant across the reactor.
- Gas–liquid mass transfer was neglected.
- For all calculations, particle diameter for all shapes was considered to be the equivalent diameter, which represent the diameter of a sphere that has the same external area as the actual particle shape.

### 2.2. Kinetic model

To develop the kinetic model experimental data of HDS reaction obtained at the following reaction conditions were utilized: 340–380 °C temperature, 1–2.5 h<sup>-1</sup> LHSV, 54 kg/cm<sup>2</sup> pressure and 2000 ft<sup>3</sup>/bbl hydrogen-to-oil ratio. A NiMo/γ-Al<sub>2</sub>O<sub>3</sub> commercial catalyst sample with tri-lobular shape was used in all experiments. Its main properties are: 2.4 wt.% Ni, 9.5 wt.% Mo, 204 m<sup>2</sup>/g specific surface area, 0.50 cm<sup>3</sup>/g pore volume, and particle density of 1.56 g/cm<sup>3</sup> (C-128-01 ASTM Method). More geometric characteristics of the 3-lobe commercial sample and of other shapes are given in Table 1. A sample of straight-run gas oil recovered from a Mexican refinery was employed as feed for all hydrodesulfurization tests. This feed has the following properties: 0.8687 specific gravity at 20/4 °C, 1.616 wt.%

total sulfur, 6.83 cSt viscosity at 40 °C, 196–407 °C distillation range (ASTM D-86 method). Detailed explanations of the experimental setup (isothermal reactor with 2.54 cm diameter), catalyst sulfiding procedure, and verification of absence of interphase gradients can be found elsewhere [10–12].

The power-law kinetic model obtained by using the experimental results during hydrodesulfurization of straight-run gas oil is:

$$-\frac{dC_A}{d(1/LHSV)} = k_{ap} C_A^n = 6.213 \times 10^{15} e^{-33940/RT} C_A^{2.4} \quad (1)$$

### 2.3. Characteristics of the catalyst bed

The bed void fraction can be calculated in the following way. This equation was developed for packed beds of spheres [13].

$$\varepsilon_B = 0.38 + 0.073 \left[ 1 + \frac{(D_R/d_{p_{eq}} - 2)^2}{(D_R/d_{p_{eq}})^2} \right] \quad (2)$$

The bed density can be evaluated from the equation [14]:

$$\rho_B = \rho_p(1 - \varepsilon_B) \quad (3)$$

The surface area of the particles per unit volume of the bed was determined with [13]:

$$a_t = \frac{6(1 - \varepsilon_B)}{d_{p_{eq}}} \quad (4)$$

Liquid and gas pressure drops can be calculated with Ergun equation [14,15]:

$$\frac{\Delta P_i}{L_B} = \frac{150(1 - \varepsilon_B)^2}{\varepsilon_B^3} \frac{u_i \mu_i}{d_{p_{eq}}^2} + \frac{1.75(1 - \varepsilon_B)}{\varepsilon_B^3} \frac{u_i^2 \rho_i}{d_{p_{eq}}} \quad (5)$$

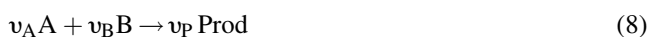
Both liquid and gas phase pressure drops can be correlated in terms of the  $\chi$  parameter. For  $0.05 < \chi < 30$  values, the following equations are employed to calculate the two-phase pressure drop in the reactor [15]:

$$\chi = \left( \frac{\Delta P_L}{\Delta P_g} \right)^{0.5} \quad (6)$$

$$\log \frac{\Delta P_{gL}}{\Delta P_g + \Delta P_L} = \frac{0.416}{0.666 + (\log \chi)^2} \quad (7)$$

### 2.4. Mass balance equations

Hydrodesulfurization of oil fractions can be considered as a bimolecular irreversible reaction between the oil (A) and hydrogen (B) reactants [16]:



The mass balance equations for the liquid and solid phases are:

- Liquid phase:

$$\frac{d(\mu_L c_{AL})}{dz} + (k_S a_t)_A (c_{AL} - c_{AS}) = 0 \quad (9)$$

- Solid phase:

$$\frac{(k_S a_t)_A (c_{AL} - c_{AS})}{v_A} = (1 - \varepsilon_B) \rho_P \eta k C_{AS}^n \quad (10)$$

For calculating  $k_S$  the following generalized correlation was used [15]:

$$\frac{k_S d_{p_{eq}}}{D_A} = 0.8 \frac{Re_L^{0.5}}{\varepsilon_L} \left( \frac{\mu_L}{\rho_L D_A} \right)^{0.333} \quad (11)$$

The liquid holdup ( $\varepsilon_L$ ) was determined with the following equation [15]:

$$\varepsilon_L = 0.185 \varepsilon_B a_t^{0.333} \chi^{0.22} \quad (12)$$

Liquid Reynolds number was evaluated with [14]:

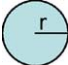
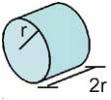

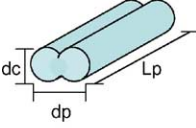
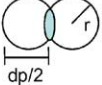
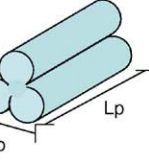
$$Re_L = \frac{d_{p_{eq}} G_L}{\mu_L} \quad (13)$$

The molecular diffusivity of solute A in the liquid is [17]:

$$D_A = 8.93 \times 10^{-8} \frac{v_L^{0.267} T}{v_A^{0.433} \mu_L} \quad (14)$$

where  $v_L$  and  $v_A$  are molar volume of solute and liquid solvent respectively, and are estimated with the following

Table 1  
Geometry of different catalyst particle shapes

	Shape	$d_p$ (cm)	$L_p$ (cm)	$d_{p_{eq}}$ (cm)	$S_p$ (cm <sup>2</sup> )	$r_c$ (cm)	$L_B/d_{p_{eq}}$
Sphere		0.314	–	0.314	0.3098	0.16	76.93
Pellet		0.274	0.274	0.274	0.3546	0.14	83.87
Cylinder		0.210	0.468	0.257	0.3780	0.11	89.42
2-Lobe		0.242	0.544	0.229	0.4234	0.074	100.16
3-Lobe		0.230	0.520	0.222	0.4381	0.058	103.62
4-Lobe		0.220	0.491	0.199	0.4878	0.046	115.40

equations [18]:

$$v_i = 0.285(v_{ci}^m \text{PM}_i)^{1.048} \quad (15)$$

$$v_c^m = 7.5214 \times 10^{-3} T_{\text{MeABP}}^{0.2896} d_{15.6}^{-0.7666} \quad (16)$$

The effectiveness factor ( $\eta$ ) in commercial hydrodesulfurization catalysts has been reported to be in the range of 0.4–0.6 [14,19–21]. These low  $\eta$  values give  $\phi > 1$  which may be considered to be within strong internal diffusional limitations [13]. This assumption will be demonstrated with further calculations of Thiele modulus. In such a case  $\eta$  becomes proportional to  $1/\phi$ :

$$\eta = \frac{1}{\phi} \quad (17)$$

The generalized Thiele modulus for  $n$ th-order irreversible reaction is [13]:

$$\phi = \frac{V_p}{S_p} \left( \frac{n+1}{2} \frac{k C_{AS}^{n-1} \rho_p}{D_e} \right)^{0.5} \quad (18)$$

Effective diffusion ( $D_e$ ) was determined with the following equation [13]:

$$D_e = \frac{\theta}{\tau} \left( \frac{1}{1/D_A + 1/D_K} \right) \quad (19)$$

Molecular diffusion is evaluated with Eq. (14) and Knudsen diffusion as follows [13]:

$$D_K = 9700 r_g \left( \frac{T}{\text{PM}} \right)^{0.5} \quad (20)$$

Catalyst porosity ( $\theta$ ) and mean pore diameter ( $r_g$ ) were calculated with the following equations from experimental data of specific surface area ( $S_g$ ), total pore volume ( $V_g$ ), and particle density ( $\rho_p$ ) and were 0.78 and 48 Å, respectively. Tortuosity factor was assumed to be 4 according to literature reports [21].

$$\theta = \rho_p V_g \quad (21)$$

$$r_g = \frac{2\theta}{S_g \rho_p} \quad (22)$$

With the value of  $\eta$  and the apparent kinetic constant given in the kinetic model (Eq. (1)), the intrinsic kinetic constant can be determined as follows [13]:

$$k = \frac{k_{ap}}{\eta} \quad (23)$$

When combining Eqs. (17), (18) and (23), the following general expression can be derived for calculating the effectiveness factor [22]:

$$\eta = \frac{2D_e(S_p/V_p)^2}{(n+1)k_{ap}C_{AS}^{n-1}\rho_p} \quad (24)$$

This equation was first used for determining the value of  $\eta$  and  $k$  for the 3-lobe extrudate commercial catalyst employed

during experiments. The intrinsic kinetic constant calculated by this way was then utilized for determining the effectiveness factor of the different particle catalyst shapes according to the following equations [5,23–25]:

- For sphere:

$$\eta = \frac{3(\phi \coth \phi - 1)}{\phi^2} \quad (25)$$

For the other shapes (pellet, cylinder, 2-lobe, 4-lobe) the following expression was employed, which has been proposed for other authors to be used for particles of irregular shape [23–25]:

$$\eta = \frac{\tanh \phi}{\phi} \quad (26)$$

## 2.5. Physical properties of oil and gas at process conditions

- Density of oil [18]:

$$\rho_L(P, T) = \rho_0 + \Delta\rho_P - \Delta\rho_T \quad (27)$$

$$\begin{aligned} \Delta\rho_P &= [0.167 + 16.181 \times 10^{-0.0425\rho_0}] \left[ \frac{P}{1000} \right] \\ &\quad - 0.01[0.299 + 263 \times 10^{-0.0603\rho_0}] \\ &\quad \times \left[ \frac{P}{1000} \right]^2 \end{aligned} \quad (28)$$

$$\begin{aligned} \Delta\rho_T &= [0.0133 + 152.4(\rho_0 + \Delta\rho_P)^{-2.45}] [T \\ &\quad - 520] - [8.1 \times 10^{-6} - 0.0622 \\ &\quad \times 10^{-0.764(\rho_0 + \Delta\rho_P)}] [T - 520]^2 \end{aligned} \quad (29)$$

- Dynamic liquid viscosity [18]:

$$\mu_L = 3.141 \times 10^{10} (T - 460)^{-3.444} [\log_{10}(\text{API})]^a \quad (30)$$

$$a = 10.313 [\log_{10}(T - 460)] - 36.447 \quad (31)$$

- Gas properties [26]:

Gas density was calculated with Redlich-Kwong equation. Gas viscosity was estimated with the following Lennard-Jones correlation [21]:

$$\mu_g = 26.693 \times 10^{-6} \frac{(\text{PM } T)^{0.5}}{\sigma^2 \Omega} \quad (32)$$

## 3. Results and discussion

### 3.1. Characteristics of particle shapes

The catalytic particles shapes used for simulation were: sphere (sph), pellet (pel), cylinder (cyl), bi-lobular (2-lobe),

tri-lobular (3-lobe), and tetra-lobular (4-lobe). Excepting for sphere shape, all the other shapes have two external areas: cross-sectional area and lateral area, which are used to calculate the total geometric external area of the particle. For cylinder and lobe-shape particles cylinders are considered symmetrical.

The geometrical characteristics ( $L_p$ ,  $d_p$ ,  $r_c$ ) of all shapes were calculated assuming that they have the same total geometric volume of the 3-lobe commercial sample ( $V_p = 0.016 \text{ cm}^3$ ) at equal  $L_p/d_p$  ratio of 2.25. For pellet shape  $L_p = d_p$  ( $L_p/d_p = 1$ ). The main characteristics of all shapes are shown in Table 1. It is observed that external area increases with the following trend and radius of cylinder behaves inversely:

$S_p$  :

sphere < pellet < cylinder < 2-lobe < 3-lobe < 4-lobe

$r_c$  : 4-lobe < 3-lobe < 2-lobe < cylinder < pellet < sphere

Table 1 also shows the  $L_B/d_{peq}$  ratio for all shapes. It is clearly seen that lobe-shape particles have higher values of this ratio, since they exhibit lower  $d_{peq}$ . If we take into account the criteria reported in the literature that at  $L_B/d_{peq} > 100$  axial dispersion can be neglected [27]. It is concluded from the values in Table 1 that to avoid deviation from plug flow behavior lobe-shape particles should be preferred.

### 3.2. Total liquid holdup

Fig. 1 presents the effect of reactor temperature on total liquid holdup for three particle shapes. The value of  $\varepsilon_L$  increases as the number of lobes in the particle is also incremented due to lower equivalent diameter, and decreases as the temperature is increased due to a reduction in the liquid density. This holdup increased with decreasing

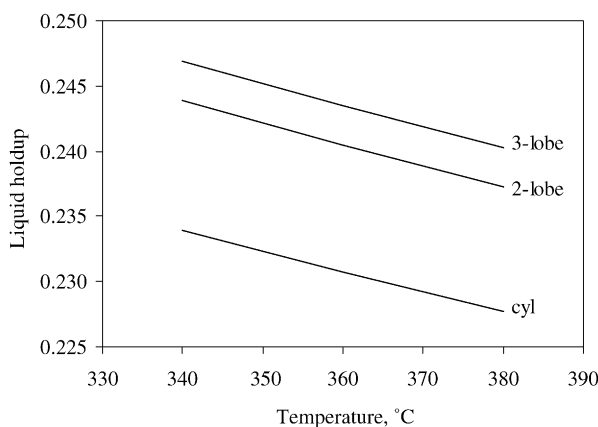


Fig. 1. Effect of reactor temperature on liquid holdup for different particle shapes ( $1.0 \text{ h}^{-1}$  LHSV).

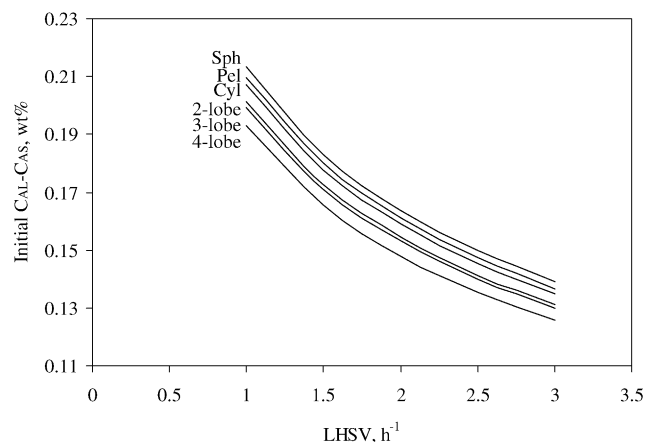


Fig. 2. Liquid–solid sulfur concentration gradients for different particle shapes and LHSV at  $340^\circ\text{C}$ .

particle size due to higher capillary pressures. This behavior has been also reported in the literature [3,28].

### 3.3. External concentration gradients

Mass transfer between liquid and solid phases is function of the liquid flow in contact with the external area of the catalytic particles, which originates a gradient between the two phases ( $C_{AL} - C_{AS}$ ). An increase of this gradient means that the reactant is not being totally transferred to the external area of the particle, which apart from the liquid flow, depends on the shape and size of the particles.

These gradients were determined in this work for different particle shapes by using the reactor model already described. As the highest gradients of concentration are found at the beginning of the catalytic bed, they were employed to magnify the differences when using different particle shapes (Fig. 2). At the same reaction conditions, it was found that the concentration gradients reduce as the

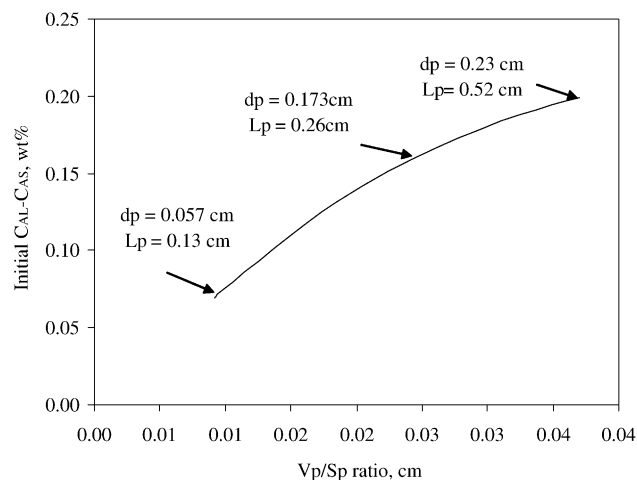


Fig. 3. Effect of particle size on liquid–solid sulfur concentration gradients (3-lobe particle shape,  $1.0 \text{ h}^{-1}$  LHSV,  $340^\circ\text{C}$ ).



external area of the particle is increased, which means that the liquid mass-transfer to the particle external area is favored by using lobe-shape particles.

The effect of  $L_p$  and  $d_p$  on external concentration gradients was examined at constant LHSV and temperature which is shown in Fig. 3 for 3-lobe shape particle. To illustrate the effect of the size of different shapes the  $V_p/S_p$  ratio was utilized. It is observed from this figure that the lower the particle size the lower the concentration gradients. This behavior implies that when small particles are used external gradients of concentration are minimal.

### 3.4. Thiele modulus

Different values of Thiele modulus were calculated for the 3-lobe commercial sample shape as a function of reactor temperature and are shown in Fig. 4. The value of  $\phi$  increases as the reactor temperature is incremented and ranges from 1.5 to 7.5. These values do not exactly represent a system with strong internal diffusion limitations, but we have assumed they are high enough to do this consideration. Hence, these values confirm the supposition given by Eq. (17) that  $\eta = 1/\phi$ .

### 3.5. Internal concentration gradients

Diffusion at the interior of the particle depends mainly on its porosity and on the size of the molecules being diffused through the pores. For comparing the effect of particle shape on internal gradients, effectiveness factors of all shapes were calculated and plotted in Fig. 5 as a function of LHSV for a reactor temperature of 340 °C. Firstly, it can be mentioned that all values are within the range reported in the literature (0.4–0.6) [14,19–21]. The lobe shapes particles yield higher effectiveness factors. It is also observed that when the number of lobes is increased higher effectiveness factor is also obtained. It means that external surface of the particle is influencing internal diffusion and consequently it can be concluded that a particle exposing higher external area facilitates internal diffusion compared with particles with

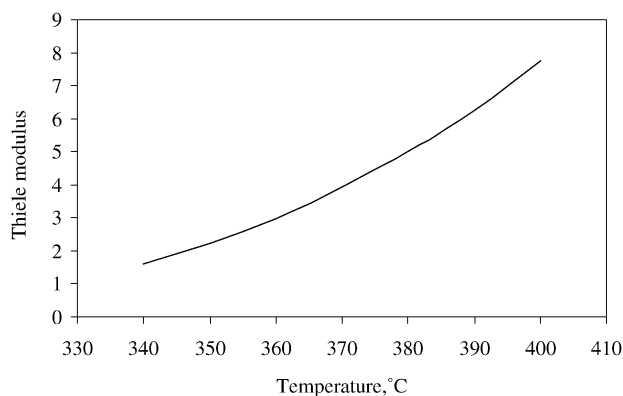


Fig. 4. Effect of temperature on Thiele modulus (3-lobe particle shape,  $1.0 \text{ h}^{-1}$  LHSV).

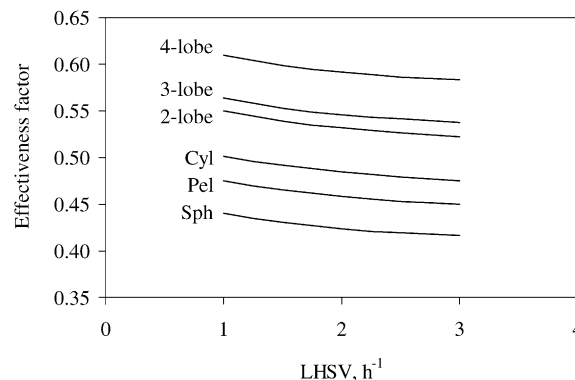


Fig. 5. Catalyst effectiveness for different particle shapes at constant  $V_p$  of  $0.016 \text{ cm}^3$  and temperature of 340 °C.

less external area for the same particle volume. Another observation from these results is that lobe-cylinder radius is diminished for the case of particles with high external area (Table 1), which reduces the internal path at the interior of the particle pores.

With respect to LHSV, it is seen that an increase in this parameter provokes a marginal reduction in the effectiveness of all particle shapes, which means that internal diffusion does not depend of the flow rates. These small differences can be attributed to external diffusion which indeed is function of flow rates. This implies that for maximum catalyst effectiveness the pilot reactor should operate with no interphase mass transfer limitations.

All these results confirm that a reduction of particle size yields an increase in particle effectiveness, and as the number of lobes is increased effectiveness is also incremented.

### 3.6. Predicted versus experimental sulfur content in products

With the reactor model described above sulfur content in products at the exit of the pilot reactor were calculated as

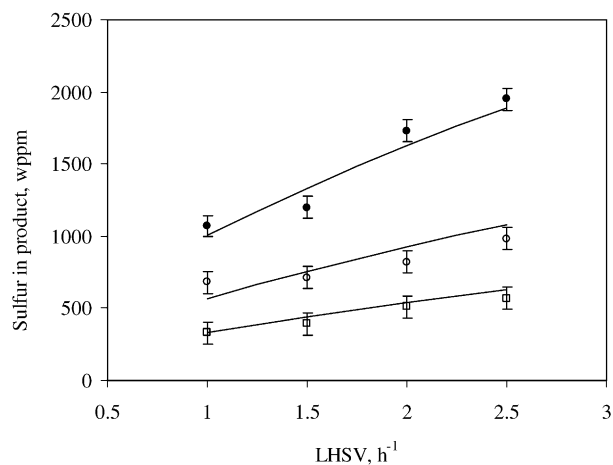


Fig. 6. Experimental (symbols) and predicted (lines) sulfur content in products. (●) 340 °C, (○) 360 °C, (□) 380 °C.

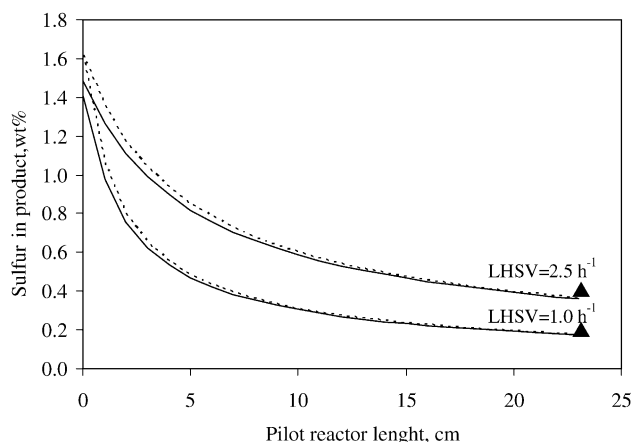


Fig. 7. Predicted (lines) and experimental (symbol) sulfur content profiles in liquid (dotted lines) and solid (solid line) phases along the experimental reactor at 340 °C.

function of reaction temperature and LHSV, which are plotted together with experimental values in Fig. 6. The average absolute error between experimental and calculated sulfur contents was lower than 4%.

The predicted sulfur content profiles at two LHSV in the experimental reactor are shown in Fig. 7. These profiles in both phases (liquid and solid) are not equal along the reactor. The gradients of concentrations between both phases are higher at the initial part of the reactor (0–5 cm) and then they are reduced further in the bed and concentrations become more or less equal. It seems that mass-transfer limitations are relatively more important at the reactor inlet, however, from certain length (~20%), diffusion and reaction resistances within the catalyst predominate. An explanation of this can be done by using the following proposed model of mass-transfer and reaction resistances, which is based on others reported in the literature [29,30]. This model neglects gas-phase resistance

$$C_{AL} = \frac{R_A}{k_L} + \frac{R_A}{k_S} + \left( \frac{R_A}{k_{ap}} \right)^{1/n} = \Delta_L + \Delta_S + \Delta_R \quad (33)$$

where  $R_A/k_L = \Delta_L$  represents the mass-transfer resistance through the gas–liquid interface,  $R_A/k_S = \Delta_S$  the resistance in the particle surface, and,  $(R_A/k_{ap})^{1/n} = \Delta_R$  the reaction resistance at the interior of the particle. One way to observe the contribution of each resistance is by means of relative resistances:

$$R_L = \frac{\Delta_L}{\Delta_T} = \frac{\Delta_L}{\Delta_L + \Delta_S + \Delta_R} \quad (34)$$

$$R_S = \frac{\Delta_S}{\Delta_T} = \frac{\Delta_S}{\Delta_L + \Delta_S + \Delta_R} \quad (35)$$

$$R_R = \frac{\Delta_R}{\Delta_T} = \frac{\Delta_R}{\Delta_L + \Delta_S + \Delta_R} \quad (36)$$

A plot of the values obtained with the above equations along the reactor is presented in Fig. 8. The behavior observed in this graph confirms that mass-transfer resistance is important

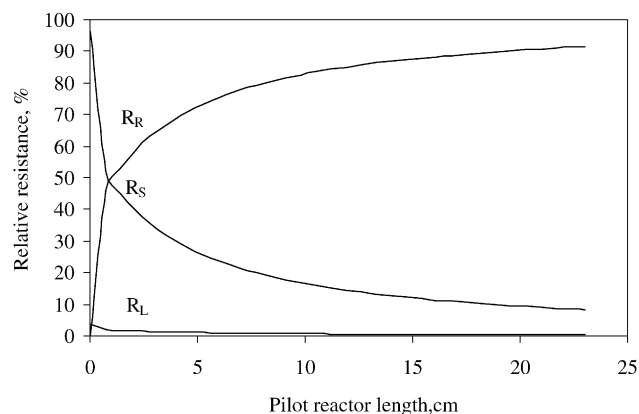


Fig. 8. Mass-transfer and reaction–diffusion relative resistances along the experimental reactor at 340 °C and 1.0 h<sup>-1</sup> LHSV.

only at the beginning of the reactor. Other works published in the literature also report similar trends with similar or different feeds [31,32].

### 3.7. Effect of the shape on sulfur content in the product

It is known that the best catalyst selected through previous screening test is formed into a shape, cylindrical or non-cylindrical, and then undergoes further experimentation for process development and optimization. At this point is where proper particle shape and size selection becomes very important, since the catalyst needs to be tested in its commercially applied size and shape in order to predict its full performance of a commercial operation rather than simple preliminary screening [7]. Consequently, the study of the effect of the catalyst shape on sulfur content in the product is more than important.

By using the reactor model, it was found that the sulfur removal was higher in 4-lobe shape compared with other shapes as can be seen in Fig. 9. The differences in hydrodesulfuration among all shapes are better observed at low severity reaction conditions, i.e. low temperature and

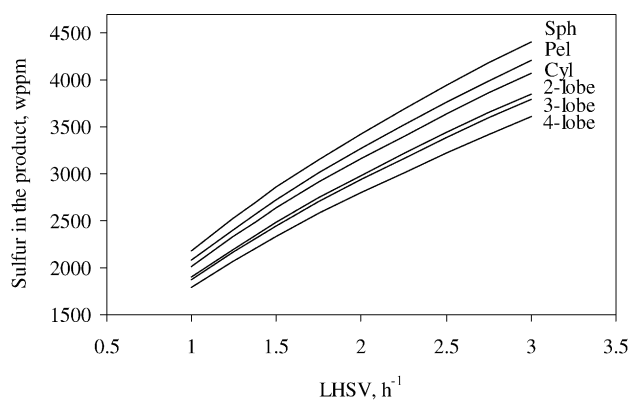


Fig. 9. Effect of LHSV on sulfur content in the product for different particle shapes at 340 °C.



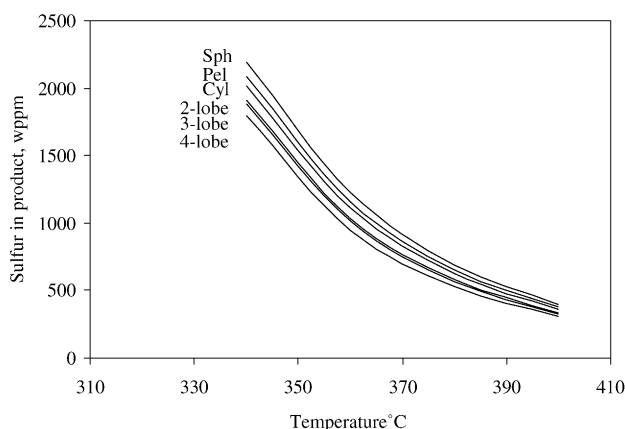


Fig. 10. Effect of temperature on sulfur content in the product for different particle shapes at  $1.0 \text{ h}^{-1}$  LHSV.

high LHSV. When reaction temperature is increased the effect of particle shape on sulfur content in the product is minimal (Fig. 10).

The impact of particle size ( $V_p/S_p$ ) on sulfur content in product is shown in Fig. 11, where it is observed that a reduction in particle size gives higher sulfur conversion, due to high effectiveness of the small particles.

Equivalent particle diameter and  $V_p/S_p$  ratio depend on each particle shape, and reduce from sphere to lobe-shape particles, for this reason non-cylindrical catalyst shapes exhibit a higher void fraction and therefore lower activities than cylindrical catalysts with equal ( $V_p/S_p$ ) are obtained.

Various simulations were carried out in order to observe the effect of changes of  $L_p$  and  $d_p$  of the particle on sulfur content in the product. The results are given in Fig. 12. It is seen that a reduction of  $d_p$  has higher effect on sulfur conversion than a reduction of  $L_p$  when they are varied the same percentage keeping one constant. This behavior is attributed to the reduction of the paths length at the interior of the particle when  $d_p$  is decremented.

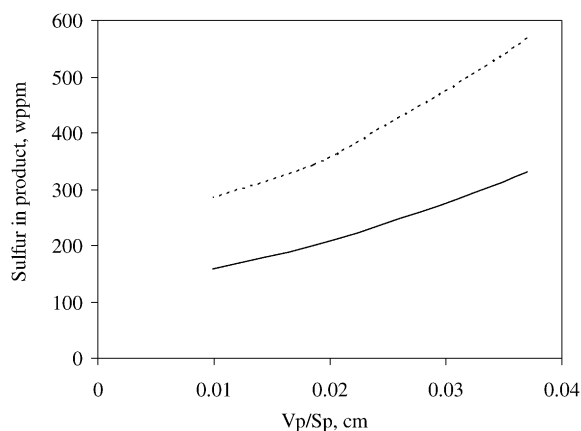


Fig. 11. Sulfur content in the product for different particle shapes as function of particle size at  $1.0 \text{ h}^{-1}$  LHSV. (---) 380 °C, (—) 400 °C.

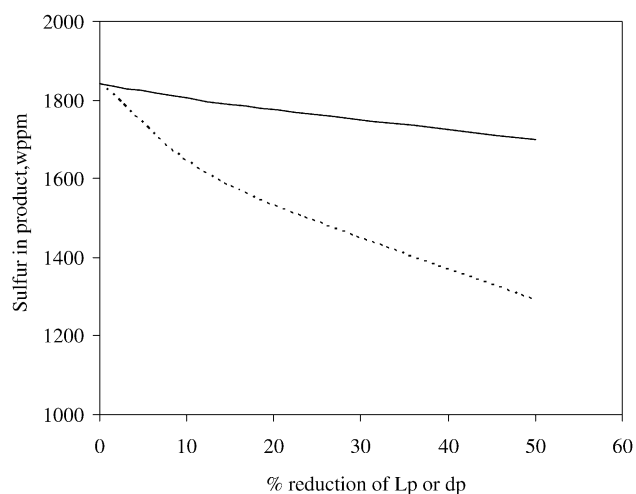


Fig. 12. Effect of reduction of particle size on sulfur content in the product for 3-lobe particle shape at  $1.0 \text{ h}^{-1}$  LHSV and 340 °C. (---) Reduction of  $d_p$  at constant  $L_p$ , (—) reduction of  $L_p$  at constant  $d_p$ .

### 3.8. Pressure drop

It is well-known that the pressure drop in the catalyst bed is related to length, diameter, shape, and bed porosity and that non-cylindrical particles exhibit lower pressure drop than others due to their higher bed porosity [2]. To demonstrate this, the effect of the different particle shapes on pressure drop was studied at constant operating conditions by varying the particle size ( $V_p/S_p$  ratio). It can be observed that the smaller the particle size the higher the pressure drop (Fig. 13). All values in Fig. 13 are plotted as the pressure drop of the particle divided by the pressure drop of the 3-lobe particle shape. These changes in pressure drop are due to the void spaces between particles in the catalytic bed [1,33].

When increasing LHSV at constant particle volume, pressure drop was incremented. This increase is due to the increment in flow velocity. Pressure drop at all LHSV was higher in lobe-shape particles.

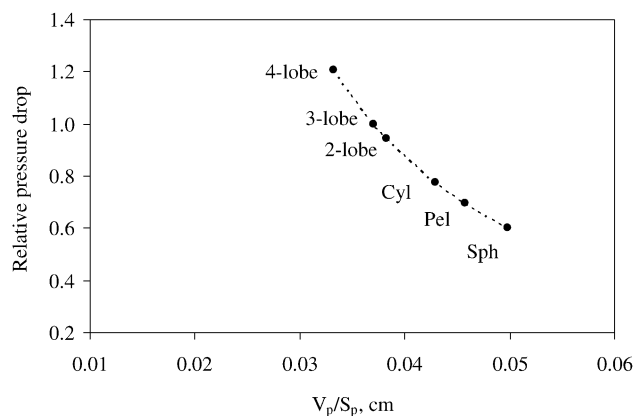


Fig. 13. Effect of particle size on relative pressure drop for different particle shapes at  $1.0 \text{ h}^{-1}$  LHSV and 340 °C.

Compared with heavy oil hydroprocessing, for middle distillates hydrodesulfurization, it is not catalyst deactivation but pressure drop which is the important factor during the commercial operation. This is the reason why catalyst strength requirements are intended to prevent pressure drop increase due to breakage. In this sense, poly-lobe particles have an acceptable strength and hence are more recommended [2].

Catalyst specifications dictate limits on the amount of small material present due to pressure drop limitation in the commercial unit. However, some small fraction invariably exists. The safest course of action is to remove the “long” material by screening prior to catalyst loading to the commercial reactor.

#### 4. Conclusions

Modeling and simulation of the small reactor studied in this work represented a good alternative to study the effect of the changes in the characteristics of both catalyst and reactor on hydrodesulfurization reaction.

The shape and size of catalyst particles will influence properties such as activity, bulk density, pressure drop, strength, and liquid distribution during commercial operation. Catalyst formulation, feed properties, and process conditions are the most relevant parameters that play an important role for determining the best geometric characteristics of catalyst particles.

#### Acknowledgments

The authors thank Instituto Mexicano del Petróleo for its financial support. M.J. Macías also thanks CONACyT for the grant during his PhD research.

#### References

- [1] B.H. Cooper, B.B.L. Donnis, B. Moyse, *Oil Gas J.* 8 (1986) 39–44.
- [2] A. de Bruijn, I. Naka, J.E.M. Sonnemans, *Ind. Eng. Chem. Proc. Des. Dev.* 20 (1981) 40–45.
- [3] J.D. Carruthers, D.J. Dicamillo, *Appl. Catal.* 43 (1988) 253–276.
- [4] S. Afandizadeh, E.A. Foumeny, *Appl. Therm. Eng.* 21 (2001) 669–682.
- [5] M. Dudukovic, *AIChE J.* 23 (1977) 940–944.
- [6] H.C. Henry, H.B. Gilbert, *Ind. Eng. Chem. Proc. Des. Dev.* 12 (1973) 328–334.
- [7] S.K. Bej, *Energy Fuels* 16 (2002) 774–784.
- [8] R. Aris, *Chem. Eng. Sci.* 6 (1957) 262–268.
- [9] T. Suzuki, T. Uchida, *Chem. Eng. Jpn.* 12 (1979) 425–429.
- [10] G. Marroquín, J. Ancheyta, *Appl. Catal. A* 207 (2001) 407–420.
- [11] J. Ancheyta, G. Marroquín, M.J. Angeles, M.J. Macías, I. Pitault, M. Forissier, R.D. Morales, *Energy Fuels* (2002) 16.
- [12] G. Marroquín, J. Ancheyta, J.A.I. Díaz, *Catal. Today* 98 (2004) 75–81.
- [13] G.F. Froment, K.B. Bischof, *Chemical Reactor Analysis and Design*, Wiley, New York, USA, 1979.
- [14] M.O. Tarhan, *Catalytic Reactor Design*, McGraw-Hill, 1983.
- [15] P.A. Ramachandran, R.V. Chaudhari, *Three Phase Catalytic Reactor*, Gordon and Breach, Science Publishers, S.A., 1983.
- [16] G. Biardi, G. Baldi, *Catal. Today* 52 (1999) 223–234.
- [17] M.P. Dudukovic, F. Larachi, P. Mills, *Catal. Rev.* 44 (2002) 123–246.
- [18] H. Korsten, U. Hoffmann, *AIChE J.* 42 (1996) 1350–1360.
- [19] D. Adlington, E. Thompson, in: *Proceedings of the Third European Symposium on Chemical Reaction and Engineering*, Amsterdam, The Netherlands, 1964, pp. 203–213.
- [20] M.P. Dudukovic, *AIChE J.* 23 (1977) 940–944.
- [21] C.N. Satterfield, *Mass Transfer in Heterogeneous Catalysis*, MIT Press, Cambridge, MA, 1970.
- [22] M.J. Macías, Estudio del efecto de las propiedades físicas de un catalizador para hidrodesulfuración mediante la modelación de un reactor de tres fases (Study of the effect of physical properties of a catalyst for hydrodesulfurization by modeling of a three-phase reactor), PhD Thesis, ESQIE-IPN, Mexico, 2004 (in Spanish).
- [23] R. Aris, *The Mathematical Theory of Diffusion and Reaction in Permeable Catalysts*, Clarendon Press, Oxford, 1975.
- [24] J. Chang, J. Liu, D. Li, *Catal. Today* 43 (1998) 233–239.
- [25] C. Li, Y.W. Chen, M.C. Tsai, *Appl. Catal. A* 34 (1995) 898–905.
- [26] J.M. Smith, H.C. Van Ness, M.M. Abbott, *Introduction to Thermodynamics in Chemical Engineering*, McGraw-Hill, 1996.
- [27] C. Perego, S. Paretello, *Catal. Today* 52 (1999) 133–145.
- [28] M.H. Al-Dahhan, M.P. Dudukovic, *Chem. Eng. Sci.* 49 (1994) 5681–5698.
- [29] O. Levenspiel, *Chemical Reaction Engineering*, 2nd ed. Wiley, New York, USA, 1986.
- [30] H.S. Fogler, *Elements of Chemical Reaction Engineering*, 3rd ed. Prentice-Hall, New Jersey, USA, 1999.
- [31] M.A. Rodríguez, J. Ancheyta, *Energy Fuels* 18 (2004) 789–794.
- [32] V. Vanrysselberghe, G.F. Froment, Hydrodesulfurization heterogeneous, in: *Encyclopedia of Catalysis*, Wiley, 2002.
- [33] A.K. Saroha, K.D.P. Nigam, Trickle bed reactors, *Rev. Chem. Eng.* 12 (1996) 207–234.